# Crystallization and Vitrification of a Cyanurate Trimer in Nanopores

Yung P. Koh and Sindee L. Simon*

Department of Chemical Engineering, Texas Tech University, P.O. Box 43121, Lubbock, Texas 79409, United States

ABSTRACT: The effects of nanopore confinement on the crystallization and vitrification of a low molecular weight organic material, tris(4-cumylphenol)-1,3,5-triazine, are investigated using differential scanning calorimetry. The material shows cold crystallization and subsequent melting in the bulk state. Under the nanoconfinement of controlled pore glasses (CPG), cold crystallization and melting shift to lower temperatures. Crystallization kinetics are hindered in nanoconfinement, and no crystallization occurs in 13 nm diameter pores over the course of a week. Using a traditional Avrami analysis, the restricted crystallization under nanopore confinement is quantified; for crystallization at 80 °C, the Avrami exponent decreases with decreasing pore size and the overall crystallization rate is approximately 30 times slower for material confined in 50 nm diameter pores than the bulk. When compared at the temperature at which the crystallization rate is a maximum, the Avrami exponent is higher in nanoconfined samples and the crystallization rate is approximately 10 times slower for material confined in 50 nm diameter pores. Under CPG nanoconfinement, the glass transition temperature also decreases and shows two values; interestingly, the T_g values further decrease with increasing crystallinity.
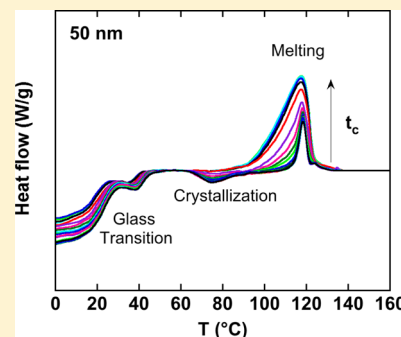
INTRODUCTION

Nanoconfinement is known to depress both freezing and melting temperatures, and reviews have been written.[1−3] The experimental observation that T_m decreases linearly with inverse crystal size[1−8] is described by the well-known Gibbs−Thomson equation.[9−11] For cylindrical confinement, the Gibbs−Thomson equation is

$$T_m = T_{m,bulk} - \frac{4T_{m,bulk}\sigma}{\Delta H_{m,bulk}\rho D} \qquad (1)$$

where T_m is the melting temperature, subscript bulk denotes T_m for the bulk material, σ is surface tension, ρ is density, D is pore diameter, and $\Delta H_{m,bulk}$ is the heat of melting of the bulk material. The equation can be derived equating the chemical potentials in solid and liquid phases accounting for the Laplace pressure which arises due to the interface surface tension.

The effects of nanoconfinement on crystallization kinetics have also been widely studied, particularly for polymeric systems in nanoconfined geometries.[12−28] The general findings for polymers confined to nanosize domains in block copolymers, in thin films, and in nanoporous matrices are that crystallization rates decrease with decreasing size of confinement, Avrami exponents decrease, and the degree of crystallinity decreases. The rate of nucleation often governs the growth of nanoconfined crystals, with a change from heterogeneous to homogeneous nucleation observed as the confinement dimension decreases;[12,14−16,19−22,24,27,28] however, for rough substrates, surface and line nucleation have been observed for polyethylene droplets,[22] whereas for polyethylene in small enough cylindrical pores or in interconnected cylinders or lamella, a return to heterogeneous nucleation has been observed.[15,16,24] A change from homogeneous to heterogeneous nucleation was also observed as film thickness decreases

for ultrathin poly(di-n-hexylsilane) films.[13] In polymeric nanocomposites, on the other hand, nanofillers often act as nucleation agents facilitating nucleation and showing higher rates of crystallization.[29−36]

In this work, the effects of nanopore confinement on the crystallization kinetics and the subsequent thermal properties of a low molecular weight organic material, tris(4-cumylphenol)-1,3,5-triazine, are examined. The material is a good glass former and has slow crystallization kinetics which allows us to easily follow isothermal crystallization in both the bulk and nanoconfined states using calorimetry. The influence of nanoconfinement and degree of crystallization on the depression of the glass transition temperature (T_g) and the melting point are also investigated. Similar to the melting point, T_g of low molecular weight glass formers is generally depressed upon nanoconfinement, and in addition, two T_g values are often observed:[2,4,37−44] one associated with material in the center of the pore, termed T_{g1}, and the other higher value associated with material at the pore surface and termed T_{g2}.[39] As a part of this work, we show that the evolution of the T_g values directly follows the evolution of crystallinity and that the T_g depression in this crystallizable system is due to both confinement in nanopores and confinement induced by the presence of crystals.

METHODOLOGY

Materials. The cyanurate trimer used in this study is tris(4-cumylphenol)-1,3,5-triazine, synthesized from monofunctional cyanate ester (4-cumylphenol cyanate, Oakwood products).

The reaction conditions used in the synthesis, 160 °C for 5 days, result in complete conversion to cyanurate trimer without degradation.[45] The chemical structure of cyanurate trimer is shown in Figure 1 (top), and the three-dimensional structure is
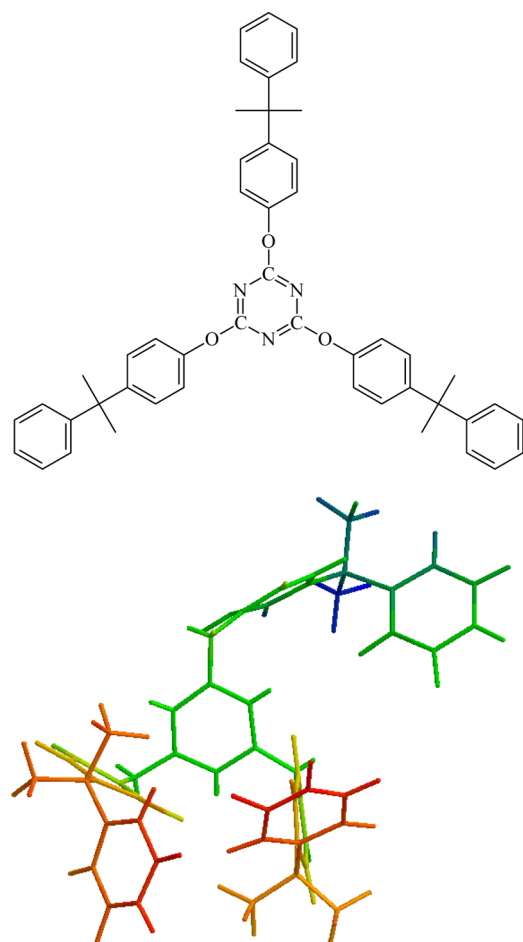

Figure 1. Chemical structure and the three-dimensional structure of cyanurate trimer in which lone electron pairs are represented by short bonds.

shown in Figure 1 (bottom); its molecular weight is 711.9 g/mol, and its density is 1.10 g/cm³ at 25 °C. The surface tension of cyanurate trimer, to be used in the Gibbs−Thomson equation, was determined to be 53.6 mJ/m² from measurement of the contact angles[46] using water and ethylene glycol solvents and silica substrate.

The nanoconfinement medium used in this study is controlled pore glass (CPG, Millipore). Three different pore sizes of CPGs are employed, ranging from 13.0 to 122.1 nm in diameter. The detailed specifications of each CPG are listed in Table 1, as provided by the manufacturer. The native CPG is made from borosilicate glass and inherently contains hydroxyl groups on its surface. Cleaning with nitric acid was followed by a silanization with hexamethyldisilazane (Sigma-Aldrich) to replace the hydrophilic hydroxyl groups with hydrophobic trimethylsilyl groups following the procedure of Jackson and McKenna.[4] The silanization treatment has been reported to result in negligible changes in pore diameter and pore size distribution.[47] The silanized CPGs were stored in a desiccator before use.

Table 1. Specifications of Controlled Pore Glasses As Provided by the Manufacturer

product name	mean pore diameter (nm)[a]	pore diameter distribution (%)[b]	specific pore volume (cm³/g)[a]	specific surface area (m²/g)[c]
CPG00130	13.0	7.4	0.68	130.0
CPG00500	50.0	3.7	1.10	50.9
CPG01200	122.1	3.7	1.73	31.2

[a]Determined by mercury intrusion method. [b]Analyzed by ultrasonic sieving method. [c]Measured by nitrogen adsorption method.

Nanoconfinement of the cyanurate trimer was achieved by imbibing the cyanate ester into the CPG pores at room temperature by placing a drop of 4-cumylphenol cyanate on the CPG. Imbibement occurs within a matter of seconds, and pores are filled to 80−90% fullness based on pore volume and 4-cumylphenol cyanate loading volume. The cyanurate trimer is then produced in situ by reaction at 160 °C for 5 days. Complete reaction occurs in the nanopores based on the fact that the heat of reaction is the same (104.1 ± 1.3 kJ/mol) as in the bulk.[45] In addition, cyanurate trimer synthesized outside the pores and then imbibed in 13 nm diameter pores shows the same T_g (18.9 ± 1.2 °C) as that synthesized inside 13 nm diameter pores.[48]

DSC Measurement. A Perkin-Elmer Pyris 1 differential scanning calorimeter (DSC) was used with an intracooler and a nitrogen atmosphere for the measurements of the glass transition, cold crystallization, and melting. All measurements were performed on heating at 10 K/min after cooling at 30 K/min. Since T_g can be obtained only on cooling by its definition,[49] here we measure the limiting fictive temperature (T_f') on heating using Moynihan's method.[50] We refer to the T_f' value as the T_g in this study since T_f' is approximately equal (within ~1 K) to the T_g value that would be obtained on cooling at the same rate.[49,51] On the other hand, the melting temperature is taken as the onset of melting from the intersection of the baseline and the tangent drawn through the steepest part of the melting transition.

Isothermal crystallization was performed in situ in the DSC since it provides good temperature control. One sample was used for all experiments in a given pore size to reduce error associated with multiple samples. Initially, a sample was heated to well above its melting temperature, held for 3 min to erase the existing thermal history, cooled to the prespecified isothermal crystallization temperature (T_c, ranging from 60 to 100 °C) at 30 K/min, partially crystallized for a prespecified time (t_c, ranging from 0 min to 7 days), cooled to −30 °C at 30 K/min, and then scanned on heating at 10 K/min back to the initial hold temperature above the melting temperature. This cycle, shown schematically in Figure 2, was repeated for various crystallization times. From the heating scans, the glass transition temperature (T_g), step change of heat capacity at T_g (ΔC_p), cold crystallization temperature (T_{cc}), melting temperature (T_m), heat of cold crystallization (ΔH_{cc}), and heat of melting (ΔH_m) were obtained as a function of isothermal crystallization time. As mentioned, isothermal crystallization studies were performed at selected temperatures between 60 and 100 °C.

The weight fraction crystallinity (X_c) is determined in two ways. First, it is determined from the step change of the heat capacity at T_g, which is related to the fraction of amorphous material:
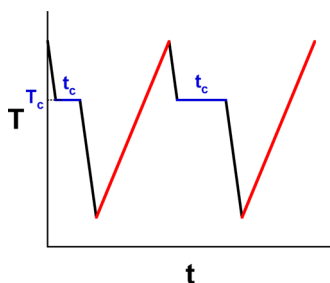
Figure 2. Schematic diagram of DSC temperature program used to study crystallization kinetics at T_c as a function of time of crystallization t_c.

$$X_c = 1 - \frac{\Delta C_P}{\Delta C_{po}} \qquad (2)$$

where ΔC_P is the step change in the heat capacity at T_g and ΔC_{po} is the step change in the heat capacity at T_g for 100% amorphous material. In addition, the weight fraction crystallinity is determined from the difference between the heat of melting and the heat of cold crystallization; since no crystallization occurs during cooling, this difference is the heat of melting associated with the material crystallized during the isothermal crystallization prior to the heating scan:

$$X_c = \frac{\Delta H_m - \Delta H_{cc}}{\Delta H_{m,tot}} \qquad (3)$$

where ΔH_m is the heat of melting, ΔH_{cc} is the heat of cold crystallization, and $\Delta H_{m,tot}$ is heat of melting for 100% crystalline material, which is determined to be 44.8 ± 4.0 J/g by equating eqs 2 and 3 for the bulk material at the maximum degree of crystallization; to the best of our knowledge, the heat of fusion for 100% crystalline tris(4-cumylphenol)-1,3,5 triazine has not been reported by other researchers.

The DSC temperature was calibrated with mercury, indium, and tin at 10 K/min on heating. The isothermal calibration, which is relevant for the isothermal crystallization temperature, was performed at 0.1 K/min, which was found in other work[52] to be equivalent to performing an isothermal calibration. The heat flow of the DSC was calibrated with indium.

■ RESULTS

The DSC heating scans for initially amorphous cyanurate trimer, in both bulk and nanopore confined states, are shown in Figure 3 (top panel) for heating immediately after cooling from 180 to −30 °C at 30 K/min. For the bulk amorphous cyanurate trimer heating trace, T_g is observed as a step change in the heat capacity at approximately 45 °C, followed by an exotherm associated with cold crystallization between 80 and 120 °C, which is immediately followed by the melting endotherm between 120 and 155 °C. The heat of cold crystallization calculated from the exotherm area is the same as the heat of melting calculated from the endotherm area, indicating that no crystallization occurred during the cooling process prior to the heating scans. As nanopore size decreases, T_g is depressed from the bulk and two T_g values are observed for all of the materials in nanopores, consistent with our previous works,[37,38,45,48,53] as well as with other works in the literature.[2,4,39−44] The cold crystallization exotherm shifts to lower temperatures for the nanoconfined samples compared to the bulk, and the temperature distance between the cold crystallization exotherm
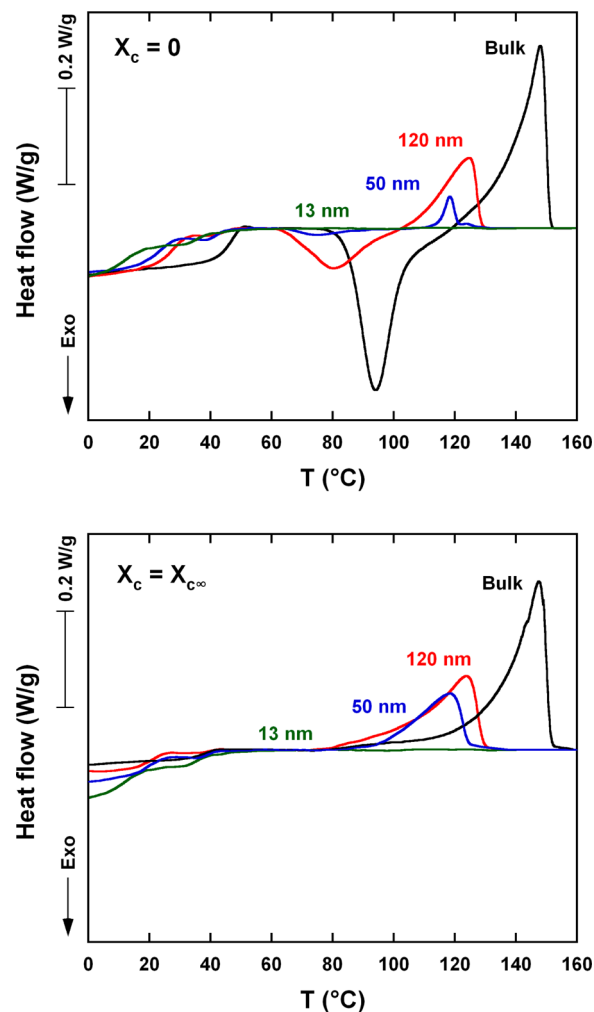

Figure 3. DSC heating scans at 10 K/min for initially amorphous material (top panel) and for crystallized material after maximal isothermal crystallization at 80 °C (bottom panel).

and the melting endotherm increases due to the decreasing rate of nanoconfined crystallization. The heats of cold crystallization and melting also decrease as nanopore size decreases, with complete suppression of crystallization in 13 nm diameter pores. Suppression of crystallization of other small molecule glass formers, namely, cyclohexane, cis-decalin,[4] benzene,[5] and *ortho*-terphenyl,[54] has been reported in the literature for nanopore confinement, and Alcoutlabi and McKenna[2] have suggested that crystallization may not occur in pores smaller than approximately 10 times the molecular size. The size of our cyanurate trimer molecule is approximately 1.25 nm; hence, the complete suppression of crystallization of cyanurate trimer in 13 nm diameter pores is consistent with this idea.

Figure 3 (bottom panel) shows the corresponding DSC heating scans for material crystallized at 80 °C to the maximum extent, both in bulk and in nanopores. The scans show first the endothermic step changes associated with the glass transition between 10 and 50 °C, with two T_g values observed in the nanoconfined systems. Since these samples were crystallized isothermally to the maximum extent prior to the heating scan, no cold crystallization is observed, and T_g is only followed by a melting peak. The melting peak shifts to lower temperatures and decreases in magnitude with confinement, the latter indicating that lower extents of crystallization are attained in the

nanopores. The decreasing degree of crystallization in the nanoconfined samples is also reflected by an increase in the magnitude of the step change in C_p at T_g since more amorphous material is present as the degree of crystallinity decreases. For the material confined in 13 nm diameter pores, the total ΔC_p (for the two steps at T_{g1} and T_{g2}) is the same as the bulk uncrystallized sample and no melting is observed, indicating that this sample is fully amorphous even after 7 days at 80 °C. In fact, as shown by eq 2, the ratio of the ΔC_p values of the maximally crystallized and amorphous cyanurate trimer is directly related to the degree of crystallinity; the maximum attainable crystallinity, $X_{c\infty}$, is calculated to be 0.76, 0.41, and 0.38 for the bulk, 120 nm confined, and 50 nm confined samples, respectively, for crystallization at 80 °C.

The evolution of the DSC heat flow curves as a function of isothermal crystallization time (t_c) at $T_c = 80$ °C is shown in Figure 4 (top panel) for the bulk sample and in Figure 4
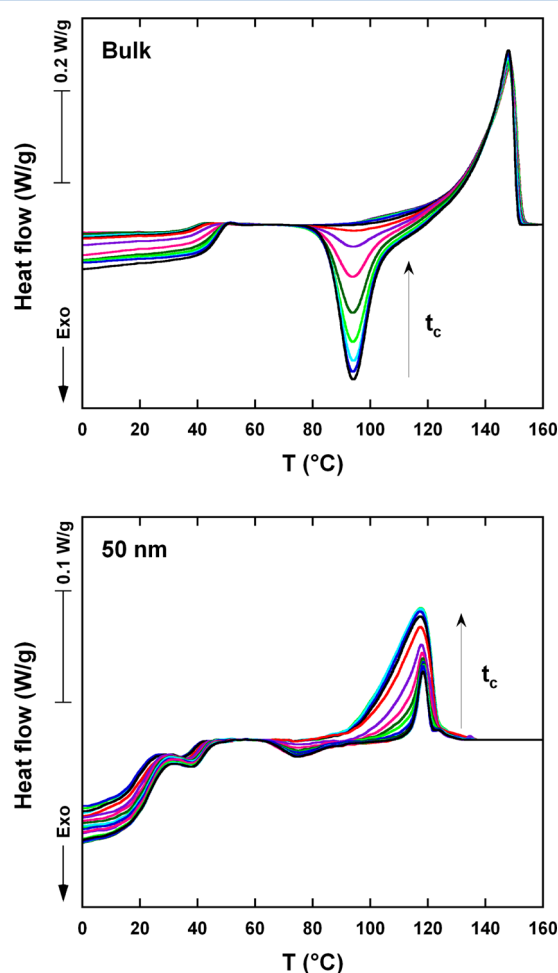

Figure 4. DSC heating scans at 10 K/min as a function of crystallization time at 80 °C for the bulk (top panel) and for samples in 50 nm diameter pores (bottom panel). Note that the *y*-axis scale differs.

(bottom panel) for the sample in 50 nm diameter pores. As crystallization proceeds, the step change in heat capacity at T_g decreases and the glass transition shifts to lower temperatures. In addition, the cold crystallization exotherm decreases in area and finally disappears at maximal crystallization, and for the nanoconfined sample, the melting endotherm increases significantly. The melting endotherm does not change for the

bulk sample as a function of the initial degree of crystallization because the partially crystallized bulk sample is able to complete crystallization during the heating scan. On the other hand, crystallization is hindered in the nanopores and its rate is slower, and consequently, maximal crystallization cannot be achieved by cold crystallization on heating; rather, only a fraction of the maximal crystallinity can be achieved during heating for an initially amorphous sample confined in nanopores, and this fraction decreases with decreasing pore size.

The Gibbs−Thomson equation can describe the size-dependent melting point[9−11] as discussed earlier. Here, we find that the Gibbs−Thomson equation with no adjustable parameters describes reasonably well the depressions of the onset melting temperature from the bulk with decreasing nanopore size, as shown in Table 2 for melting points for

Table 2. Transition Temperatures after Reaching Maximal Crystallinity at $T_c = 80$ °C

	$T_{m,onset}$ (°C)		T_g (°C)	
	exp.	G−T eq[a]	T_{g1}	T_{g2}
bulk	134.7	134.7	39.3	NA
120 nm	103.5	120.2	21.1	41.2
50 nm	95.0	99.2	17.9	40.5

[a]Calculated for $\sigma = 53.6$ mJ/m^2, $\Delta H = 44.8$ J/g, and $\rho = 1.10$ g/cm^3.

samples which have achieved maximal crystallinity at $T_c = 80$ °C. The experimental values are lower than those predicted by the Gibbs−Thomson equation presumably because of crystal imperfection and/or because crystals do not completely fill and thus are smaller than the pores. Also shown in Table 2 are the T_g values after maximal crystallization is achieved; the change of T_g with crystallinity will be discussed later.

The kinetics of crystallization can be determined from the change in crystallinity (X_c) as a function of isothermal crystallization time (t_c). In Figure 5, the evolution of crystallinity is plotted for the bulk sample, along with samples
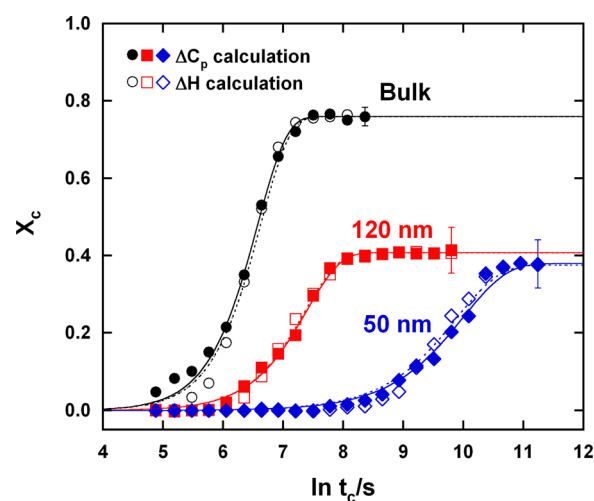

Figure 5. Evolution of the degree of crystallinity as a function of crystallization time t_c at $T_c = 80$ °C. The filled symbols represent the degree of crystallinity calculated from ΔC_p, and the open symbols represent the degree of crystallinity calculated from the heats of cold crystallization and melting. The corresponding Avrami fits are solid and dotted lines, respectively.

Table 3. Avrami Fitting Results, Half Time of Crystallization, and Maximum Attainable Crystallinity of the Bulk Crystallization and the Nanoconfined Crystallization in 120 and 50 nm Diameter Pores at T_c = 80 °C

	bulk		120 nm		50 nm	
	ΔC_p data	ΔH data	ΔC_p data	ΔH data	ΔC_p data	ΔH data
n	1.97 ± 0.25	2.57 ± 0.27	1.79 ± 0.38	1.76 ± 0.49	1.43 ± 0.38	1.52 ± 0.34
k (10^{-6} s^{-n})	2.44 ± 0.27	0.0459 ± 0.0037	1.70 ± 0.28	2.44 ± 0.49	0.578 ± 0.129	0.320 ± 0.068
K (10^{-4} s^{-1})	14.0 ± 0.8	13.9 ± 0.5	6.07 ± 0.56	6.52 ± 0.65	0.446 ± 0.056	0.534 ± 0.043
$t_{1/2}^{-1}$ (10^{-4} s^{-1})	16.9	16.0	7.45	8.02	0.575	0.679
$X_{c\infty}$	0.76 ± 0.02		0.41 ± 0.06		0.38 ± 0.06	

in 120 and 50 nm diameter pores, for T_c = 80 °C. X_c is determined in two ways: the filled symbols are based on the step change in heat capacity at T_g (eq 2), whereas the open symbols show X_c calculated from the heats of cold crystallization and melting (eq 3); the two methods are in good agreement. Under nanopore confinement, the rate of crystallization and the maximum attainable crystallization decrease, consistent with the results shown in Figures 3 and 4. To be more specific, crystallization is delayed by a factor of approximately 30 in 50 nm pores compared to the bulk, and the maximum degree of crystallinity decreases from 0.76 to 0.38.

The effects of nanoconfinement on the rate of crystallization are quantified in more detail using a traditional Avrami analysis:[55,56]

$$X_c/X_{c\infty} = 1 - \exp[-kt^n] = 1 - \exp[-(Kt)^n] \qquad (4)$$

where X_c is mass fraction crystallinity, $X_{c\infty}$ is the maximum attainable crystallinity, k is the rate constant in units of time^{-n}, K is the rate constant in units of time^{-1}, and n is the Avrami exponent. The k is a function of both temperature and Avrami exponent n, whereas K ($=k^{1/n}$) is independent of n. Note that k and n depend on both geometry and nucleation, and although n should be an integer based on the original derivation, it is found to be non-integer for most materials.[56] The original Avrami equation was derived in terms of volume fraction crystallinity v_c, but weight fraction crystallinity X_c can be used and is used in the present work.

The fits to the Avrami equation are shown in Figure 5 as solid and dotted lines for degree of crystallinity calculated from heat capacity and enthalpy calculations, respectively. The Avrami equation describes the experimental data well, and the resulting fitting parameters are summarized in Table 3. The Avrami exponent n decreases with decreasing pore size from a value near 2.0 in the bulk to 1.5 in the 50 nm diameter pores, indicating that the dimension of crystal growth at the nanoscale is reduced or that crystallization becomes more dominated by homogeneous nucleation (n = 1). Reduced Avrami exponents under nanoconfinement have been reported for polyethylene domains confined in block copolymers,[12−16] for polyethylene and polypropylene in nanoporous alumina,[23] and for ultrathin films of poly(di-n-hexylsilane), poly(ethylene terephthalate), and poly(3-hydroxybutyrate).[13,18,26] The reciprocal half time ($1/t_{1/2}$) of crystallization is also shown in Table 3 and has been used to quantify the rate of crystallization in the literature. The effects of nanoconfinement on the reciprocal half time of crystallization and the modified rate constant K are consistent. The overall crystallization rate at 80 °C, characterized by the reciprocal half time of crystallization and the modified Avrami rate constant K, is approximately 4−5 times slower than the bulk, based on ΔC_p and ΔH data, respectively, for samples confined in 120 nm diameter pores, whereas the crystallization is 30−26 times slower, based on ΔC_p and ΔH data,

respectively, for samples confined in 50 nm diameter pores. Reductions in crystallization rates have similarly been observed for nanoconfined polyethylene, polypropylene, poly(ethylene oxide), poly(ethylene terephthalate), poly(caprolactone), poly-(di-n-hexylsilane), and poly(3-hydroxy butyrate).[12−15,17,18,20,24−28]

As crystallization proceeds, the step change in the heat capacity at T_g decreases in proportion to the decrease in the amorphous fraction, as shown in Figure 4, and concomitantly, the T_g values decrease with increasing crystallinity. Using the same parameters which described the crystallization kinetics, we can describe the evolution in the T_g values by applying an Avrami-type equation to the T_g depression:

$$\Delta T_g = \Delta T_{g\infty}(1 - \exp[-kt^n]) \qquad (5)$$

where ΔT_g is the change in T_g from the amorphous state, $\Delta T_{g\infty}$ is the change in T_g at maximal crystallinity, k is the rate constant, and n is the Avrami exponent. The changes in the T_g values as a function of crystallization time at 80 °C are shown in the top and bottom panels of Figure 6 for T_{g1} and T_{g2}, respectively, with solid and dotted lines using the values of the Avrami parameters based on ΔC_p and ΔH data, respectively. The fact that the Avrami-type equation using the fitting parameters from the $X_c(t)$ data describes the evolution of the T_g depression provides evidence that T_g and crystallinity are directly related; that is, the decrease in T_g in the crystallizing system is due to an increase in the magnitude of nanoconfinement imposed by the increase in crystallinity. The importance of the finding shown in Figure 6 is its seeming lack of consistency with the argument that mobility at surfaces and interfaces[57−61] is the sole cause of the T_g depression—in this system, amorphous material at the interface with crystalline material might be expected to be more constrained (less mobile), and yet the amorphous phase shows a reduced T_g (higher segmental mobility) with increasing crystallinity. However, the assumption that the crystalline domains have lower local mobility may be incorrect given the local mobility in Glotzer's quasi-crystalline phases of non-interacting particles.[62]

In our previous study of the reaction kinetics of cyanate ester to cyanurate trimer in 13 nm diameter pores,[45] the evolution of $T_{g2} - T_{g1}$ as a function of conversion was found to be constant at 28.7 ± 2.2 °C, independent of reaction temperature and conversion, backing up the previous assertion[48] that the surface layer mobility (T_{g2}) is dominated by the mobility in the adjacent core (T_{g1}). Here, we further examine the evolution of $T_{g2} - T_{g1}$ for the cyanurate trimer as a function of degree of crystallinity, as shown in Figure 7. The values of $T_{g2} - T_{g1}$ are 19.8 ± 0.9 °C for 120 nm diameter pores and 22.8 ± 0.2 °C for 50 nm diameter pores, independent of the degree of crystallization. As mentioned, for amorphous material in 13 nm diameter pores, $T_{g2} - T_{g1} = 28.7$ °C. Although there seems to be an effect of pore size on the value of $T_{g2} - T_{g1}$,[53] the
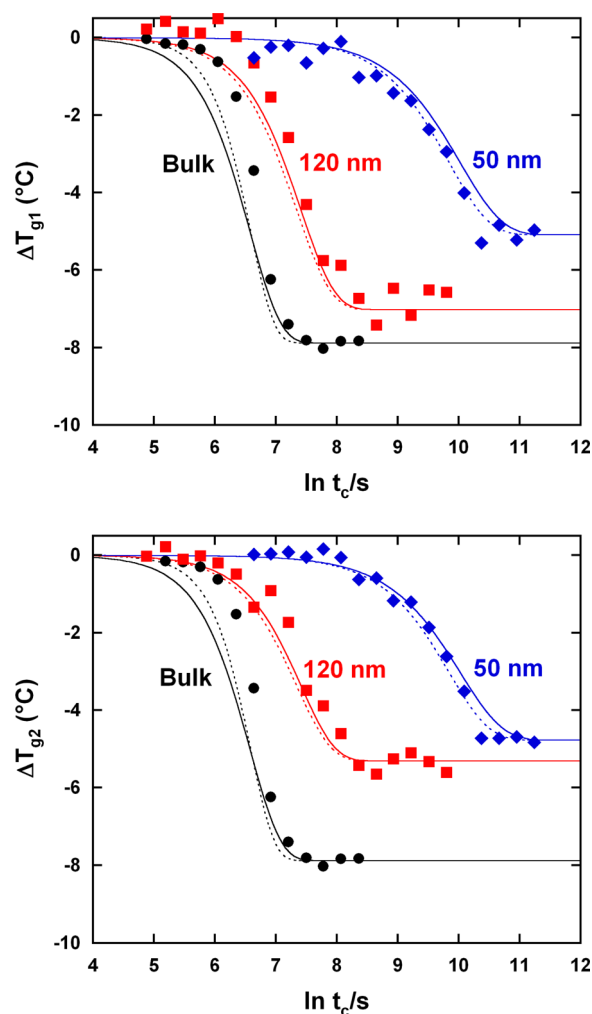
Figure 6. T_g depression from the amorphous state, $\Delta T_g = T_g(X_c) - T_g(X_c = 0)$, as a function of the crystallization time at $T_c = 80$ °C for T_{g1} (top panel) and for T_{g2} (bottom panel). The solid and dotted lines are the Avrami-type equation with parameter values from $X_c(t)$ (Figure 5) calculated from ΔC_p and from the heats of cold crystallization and melting, respectively.
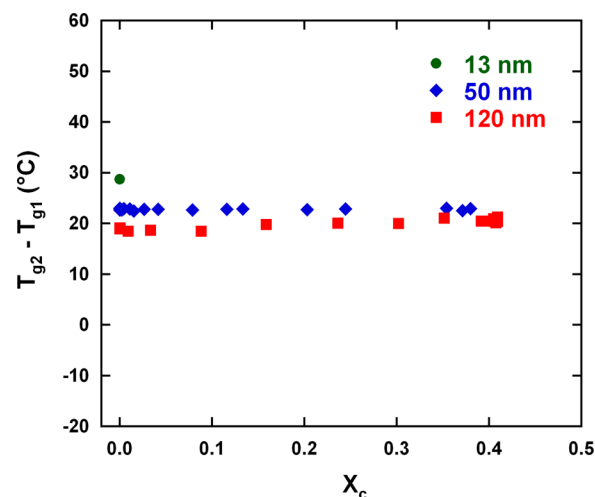

Figure 7. Difference $T_{g2} - T_{g1}$ as a function of the degree of crystallinity for crystallization at 80 °C. The data of cyanurate trimer in 13 nm diameter pores at zero crystallinity are added from our previous work.[45]
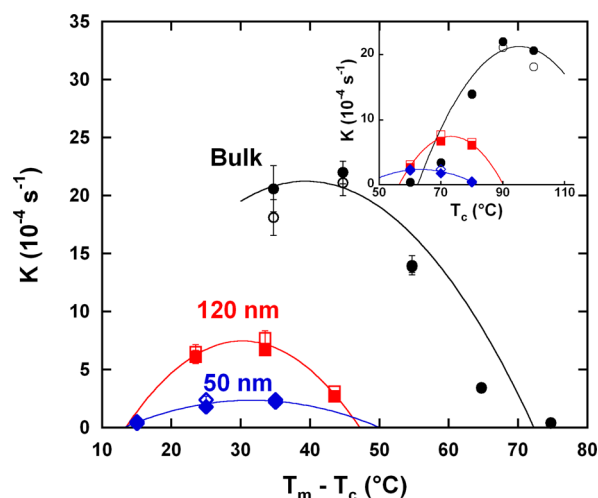

Figure 8. Dependence of the modified Avrami rate constant K on $T_m - T_c$ and, in the inset, versus T_c. The filled symbols represent the data from ΔC_p, and the open symbols represent the data from the heats of cold crystallization and melting. Lines are guides for the eye only.

results are consistent with the surface layer mobility (reflected by T_{g2}) being dominated by the mobility in the adjacent core (reflected by T_{g1}). In addition, the calculated surface layer thickness in the pores is also independent of the degree of crystallization within experimental error, being 1.6 ± 0.2 and 1.7 ± 0.3 nm for 50 and 120 nm diameter pores, respectively, consistent with our previous surface layer thickness of 1.2 ± 0.1 nm for various pore sizes from 8.1 to 122.1 nm.[45,48] The unchanged surface thickness is a reflection of the fact that, as degree of crystallization increases, total ΔC_p ($\Delta C_{p1} + \Delta C_{p2}$) decreases due to decreasing amorphous fraction, but the ratio of ΔC_{p1} and ΔC_{p2} remains constant.

All of the results reported thus far have been for isothermal crystallization at 80 °C. Here, we examine the dependence of the crystallization kinetics on T_c. The dependence of crystallization rate on T_c is shown in Figure 8, where the modified Avrami rate constant (K) is plotted versus $T_m - T_c$, with the inset plotted versus T_c. A maximum in crystallization rate is observed at approximately 35−40 K below T_m, midway between T_m and T_g, for all samples. This behavior is the general observation for polymer materials and small molecules[63] where

the overall rate of crystallization is determined by competition between the nucleation rate (which increases with decreasing T_c) and the growth rate (which increases with increasing T_c). The absolute temperature of the maximum, shown in the inset, is near the cold crystallization peak temperature observed in Figure 3 (top) and decreases with decreasing pore size, reflecting the change in the melting point. Also clearly shown in Figure 8 is the reduced crystallization rate for the nanoconfined samples. At the maximum crystallization temperature, we find that in 50 nm diameter pores, the crystallization rate decreases by a factor of approximately 10, compared to the value of approximately 30 found when comparing rates at the same crystallization temperature, $T_c = 80$ °C.

The effect of crystallization temperature on the Avrami exponent n is shown in Figure 9 as a function of $T_m - T_c$. For the bulk, the Avrami exponent n decreases with increasing T_c and then levels off at a value of approximately 2.0. The nanoconfined samples in both 120 and 50 nm diameter pores similarly show n decreasing with increasing T_c, but the
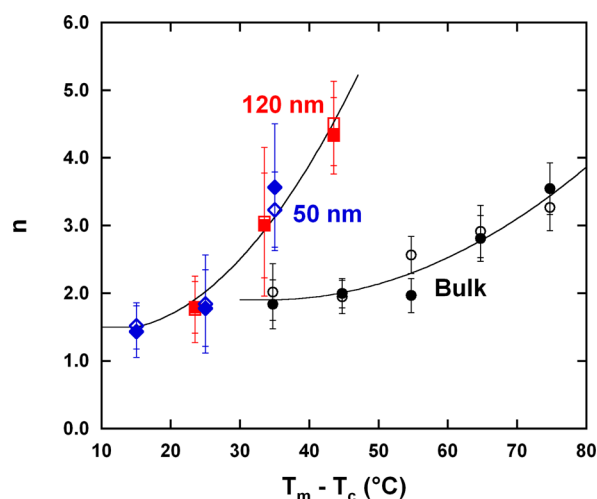

Figure 9. Dependence of the Avrami exponent n on $T_m - T_c$. The filled symbols represent the data from ΔC_p, and the open symbols represent the data from the heats of cold crystallization and melting. Lines are guides for the eye only.

dependence is stronger and seems to level off at a value of approximately 1.5, and both sets of nanoconfined data superpose when plotted versus $T_m - T_c$. The decreasing value of n with increasing temperature for both bulk and nanoconfined samples indicates that nucleation is not homogeneous, even for our nanoconfined samples; this result presumably arises because crystallization is not isolated within the pores of the CPG matrix due to pore connectivity, and this is consistent with results for ultrathin poly(di-n-hexylsilane) films,[13] for polyethylene in cylindrical nanopores,[24] and for polyethylene confined to lamellar and interconnected cylindrical domains in block copolymers.[15,16] Although crystallization kinetics are a strong function of crystallization temperature, the maximum degree of crystallinity ($X_{c\infty}$) appears to be independent of T_c within experimental error for both bulk and nanoconfined samples, as summarized in Table 4.

Table 4. Maximum Attainable Crystallinity ($X_{c\infty}$) of the Bulk Crystallization and the Nanoconfined Crystallization in 120 and 50 nm Diameter Pores as a Function of T_c

T_c (°C)	bulk	120 nm	50 nm
60	0.76 ± 0.02	0.56 ± 0.04	0.39 ± 0.06
70	0.74 ± 0.03	0.48 ± 0.05	0.46 ± 0.05
80	0.76 ± 0.02	0.41 ± 0.06	0.38 ± 0.06
90	0.72 ± 0.03		
100	0.70 ± 0.03		

■ CONCLUSIONS

The kinetics of crystallization of a cyanurate trimer (tris(4-cumylphenol)-1,3,5-triazine) under nanopore confinement were investigated using DSC. Nanoconfinement results in both a reduction in the crystallinity and a reduction in the crystallization rate compared to the bulk, with no crystallization observed in 13 nm diameter pores. Crystallization kinetics were quantified using the Avrami equation; for crystallization at 80 °C in 50 nm diameter pores, the modified Avrami rate constant K is approximately 30 times lower than the bulk, and the Avrami exponent n is reduced to a value of approximately 1.5 from the bulk value of 2.0. All samples show a maximum in

crystallization rate at approximately $T_c = T_m - 35$ K, and even when compared at this temperature, crystallization is approximately 10 times slower in 50 nm diameter pores relative to the bulk. The value of n also decreases with increasing crystallization temperature, whereas the maximum degree of crystallinity is found to be independent of T_c.

The glass transition temperature is depressed upon nanoconfinement and shows two T_g values in the CPG nanopores. The T_g values further decrease with increasing crystallinity. The evolution of T_g is well described by the Avrami-type equation with parameters from $X_c(t)$, providing evidence that T_g and the degree of crystallinity are directly related; that is, the decrease in T_g in the crystallizing system is due to an increase in the magnitude of nanoconfinement imposed by the increase in crystallinity. This result seems to be inconsistent with interfacial mobility being the sole cause of the T_g depression in these nanoconfined glasses.

■ AUTHOR INFORMATION

Corresponding Author
*E-mail: sindee.simon@ttu.edu.

Notes
The authors declare no competing financial interest.

■ ACKNOWLEDGMENTS

■ REFERENCES

(1) Alba-Simionesco, C.; Coasne, B.; Dosseh, G.; Dudzidak, G.; Gubbins, K. E.; Randhakrishnan, R.; Sililinska-Bartkowiak, M. *J. Phys.: Condens. Matter* **2006**, *18*, R15−R68.
(2) Alcoutlabi, M; McKenna, G. B. *J. Phys.: Condens. Matter* **2005**, *17*, R461−R524.
(3) Christenson, H. K. *J. Phys.: Condens. Matter* **2001**, *13*, R95−R133.
(4) Jackson, C. L.; McKenna, G.. B. *J. Chem. Phys.* **1990**, *93*, 9002−9011.
(5) Morineau, D.; Xia, Y.; Alba-Simionesco, C. *J. Chem. Phys.* **2002**, *117*, 8966−8972.
(6) Alba-Simionesco, C.; Dosseh, G.; Dumont, E.; Frick, B.; Geil, B.; Morineau, D.; Teboul, V.; Xia, Y. *Eur. Phys. J. E* **2003**, *12*, 19−28.
(7) Bassett, D. C.; Davitt, R. *Polymer* **1974**, *15*, 721−728.
(8) Sun, J.; Simon, S. L. *Thermochim. Acta* **2007**, *463*, 32−40.
(9) Gibbs, J. W. *Collected Works*; Yale University Press: New York, 1928; pp 314−331.
(10) Thomson, W. *Philos. Mag.* **1871**, *42*, 448−452.
(11) Defay, R.; Rrigogine, I.; Bellemans, A.; Everett, D. H. *Surface Tension and Adsorption*; Longmans: London, 1966; pp 310−348.
(12) Lotz, B.; Kovacs, A. J. *ACS Polym. Prepr.* **1969**, *10*, 820−825.
(13) Despotopoulou, M. M.; Frank, C. W.; Miller, R. D.; Rabolt, J. F. *Macromolecules* **1996**, *29*, 5797−5804.
(14) Loo, Y. L.; Register, R. A.; Ryan, A. J. *Phys. Rev. Lett.* **2000**, *84*, 4120−4123.
(15) Loo, Y. L.; Register, R. A.; Ryan, A. J.; Dee, G. T. *Macromolecules* **2001**, *34*, 8968−8977.
(16) Loo, Y. L.; Register, R. A.; Ryan, A. J. *Macromolecules* **2002**, *35*, 2365−2374.
(17) Sun, L.; Zhu, L.; Ge, Q.; Quirk, R. P.; Xue, C.; Cheng, S. Z. D.; Hsiao, B. S.; Avila-Orta, C. A.; Sics, I.; Cantino, M. E. *Polymer* **2004**, *45*, 2931−2939.
(18) Zhang, Y.; Lu, Y. G.; Duan, Y. X.; Zhang, J. M.; Yan, S. K.; Shen, D. Y. *J. Polym. Sci., Part B: Polym. Phys.* **2004**, *42*, 4440−4447.
(19) Lorenzo, A. T.; Arnal, M. L.; Muller, A. J.; de Fierro, A. B.; Abetz, V. *Eur. Polym. J.* **2006**, *42*, 516−533.
(20) Sun, Y. S.; Chung, T. M.; Li, Y. J.; Ho, R. M.; Ko, B. T.; Jeng, U. S.; Lotz, B. *Macromolecules* **2006**, *39*, 5782−5788.

(21) Massa, M. V.; Carvalho, J. L.; Dalnoki-Veress, K. *Phys. Rev. Lett.* **2006**, *97*, 247802−24785.

(22) Carvalho, J. L.; Dalnoki-Veress, K. *Phys. Rev. Lett.* **2010**, *105*, 237801−237804.

(23) Shin, K.; Woo, E.; Jeong, Y. G.; Kim, C.; Huh, J.; Kim, K.-W. *Macromolecules* **2007**, *40*, 6617−6623.

(24) Woo, E.; Huh, J.; Jeong, Y. G.; Shin, K. *Phys. Rev. Lett.* **2007**, *98*, 136103−136106.

(25) Napolitano, S.; Wübbenhorst, M. *Macromolecules* **2006**, *39*, 5967.

(26) Napolitano, S.; Wübbenhorst, M. *J. Phys.: Condens. Matter* **2007**, *19*, 205121−205129.

(27) Chung, T.-M.; Wang, T.-C.; Ho, R.-M.; Sun, Y.-S.; Ko, B.-T. *Macromolecules* **2010**, *43*, 6237−6240.

(28) Duran, H.; Steinhart, M.; Butt, H.-J.; Floudas, G. *Nano Lett.* **2011**, *11*, 1671−1675.

(29) Ke, Y. C.; Long, C. F.; Qi, Z. N. *J. Appl. Polym. Sci.* **1999**, *71*, 1139−1146.

(30) Hambir, S.; Bulakh, N.; Kodgire, P.; Kalgaonkar, R.; Jog, J. P. *J. Polym. Sci., Part B: Polym. Phys.* **2001**, *39*, 446−450.

(31) Hambir, S.; Bulakh, N.; Jog, J. P. *Polym. Eng. Sci.* **2002**, *42*, 1800−1807.

(32) Priya, L.; Jog, J. P. *J. Polym. Sci., Part B: Polym. Phys.* **2002**, *40*, 1682−1689.

(33) Priya, L.; Jog, J. P. *J. Polym. Sci., Part B: Polym. Phys.* **2003**, *41*, 31−38.

(34) Grady, B. P.; Pompeo, F.; Shambaugh, R. L.; Resasco, D. E. *J. Phys. Chem. B* **2002**, *106*, 5852−5858.

(35) Kodjie, S. L.; Li, L. Y.; Li, B.; Cai, W.; Li, C. Y.; Keating, M. *J. Macromol. Sci., Part B: Phys.* **2006**, *45*, 231−245.

(36) Dillon, D. R.; Tenneti, K. K.; Li, C. Y.; Ko, F. K.; Sics, I.; Hsiao, B. S. *Polymer* **2006**, *47*, 1678−1688.

(37) Li, Q. X.; Simon, S. L. *Macromolecules* **2008**, *41*, 1310−1317.

(38) Li, Q. X.; Simon, S. L. *Macromolecules* **2009**, *42*, 3573−3579.

(39) Arndt, M.; Stannarius, R.; Gorbatschow, W.; Kremer, F. *Phys. Rev. E* **1996**, *54*, 5377−5390.

(40) Schonhals, A.; Goering, H.; Schick, C.; Frick, B.; Zorn, R. *Colloid Polym. Sci.* **2004**, *282*, 882−891.

(41) Schuller, J.; Richert, R.; Fischer, E. *Phys. Rev. B* **1995**, *52*, 15232−15238.

(42) Patkowski, A.; Ruths, T.; Fischer, E. *Phys. Rev. E* **2003**, *67*, 021501−021508.

(43) Streck, C.; Mel'nichenko, Y. B.; Richert, R. *Phys. Rev. B* **1996**, *53*, 5341−5347.

(44) Park, J. Y.; McKenna, G. B. *Phys. Rev. B* **2000**, *61*, 6667−6676.

(45) Koh, Y. P.; Simon, S. L. *J. Phys. Chem. B* **2011**, *115*, 925−932.

(46) Wu, S. *J. Polym. Sci. Polym. Symp.* **1971**, *34*, 19−25.

(47) Erb, V. Diploma Thesis, Max-Planck-Institut fur Polymerforschung, Mainz, Germany, 1993.

(48) Koh, Y. P.; Simon, S. L. *J. Phys. Chem. B* **2010**, *114*, 7727−7734.

(49) Badrinarayanan, P.; Zheng, W.; Li, Q.; Simon, S. L. *J. Non-Cryst. Solids* **2007**, *353*, 2603−2612.

(50) Moynihan, C. T.; Macedo, P. B.; Montrose, C. J.; Gupta, P. K.; DeBolt, M. A.; Dill, J. F.; Dom, B. E.; Drake, P. W.; Easteal, A. J.; Elterman, P. B.; Moeller, R. P.; Sasabe, H.; Wilder, J. A. *Ann. NY Acad. Sci.* **1976**, *279*, 15−35.

(51) Plazek, D. J.; Frund, Z. N. *J. Polym. Sci., Part B: Polym. Phys.* **1990**, *28*, 431−448.

(52) Simon, S. L.; Sobieski, J. W.; Plazek, D. J. *Polymer* **2001**, *42*, 2555.

(53) Koh, Y. P.; Li, Q. X.; Simon, S. L. *Thermochim. Acta* **2009**, *492*, 45−50.

(54) Jackson, C. L.; McKenna, G. B. *Chem. Mater.* **1996**, *8*, 2128−2137.

(55) Avrami, M. *J. Chem. Phys.* **1939**, *7*, 1103−1112.

(56) Wunderlich, B. *Thermal Analysis of Polymeric Materials*; Springer: Berlin, 2005; pp 255−278.

(57) Forrest, J. A.; Dalnoki-Veress, K. *Adv. Colloid Interface Sci.* **2004**, *94*, 167−196.

(58) Forrest, J. A.; Mattsson, J. *J. Phys. IV* **2000**, *10*, 251−254.

(59) Forrest, J. A.; Dalnoki-Veress, K.; Dutcher, J. R. *Phys. Rev. E* **1997**, *56*, 5705−5716.

(60) Ellison, C. J.; Torkelson, J. M. *Nat. Mater.* **2003**, *2*, 695−700.

(61) Sharp, J. S.; Forrest, J. A. *Phys. Rev. Lett.* **2003**, *91*, 235701−235704.

(62) Damasceno, P. E.; Engel, M.; Glotzer, S. C. *ACS Nano* **2012**, *6*, 609−614.

(63) Magill, J. H.; Plazek, D. J. *J. Chem. Phys.* **1967**, *46*, 3757−3769.